

# Vectorial and spinorial perturbations in Galileon Black Holes: Quasinormal modes, quairesonant modes and stability

E. Abdalla\*

*Instituto de Física, Universidade de São Paulo,  
Caixa Postal 66318, 05314-970, São Paulo, São Paulo , Brazil*

B. Cuadros-Melgar†

*Escola de Engenharia de Lorena, Universidade de São Paulo,  
Estrada Municipal do Campinho S/N,  
Bairro Campinho, 12602-810, Lorena, São Paulo, Brazil*

Jeferson de Oliveira‡

*Instituto de Física, Universidade Federal de Mato Grosso,  
78060-900, Cuiabá, Mato Grosso, Brazil*

A. B. Pavan§

*Instituto de Física e Química, Universidade Federal de Itajubá,  
Caixa Postal 50, 37500-903, Itajubá, Minas Gerais, Brazil*

C. E. Pellicer¶

*Escola de Ciências e Tecnologia, Universidade Federal do Rio Grande do Norte,  
Caixa Postal 1524, 59072-970, Natal, Rio Grande do Norte, Brazil*

## Abstract

In this work we have considered a model that includes the interaction of gravity and matter fields with Galilean invariance (the so-called derivative coupling) as well as some corresponding black hole type solutions. Quasinormal perturbations of two kinds of matter fields have been computed by different methods. The effect of the derivative coupling in the quasinormal spectrum has been analyzed and evaluated.

---

\* eabdalla@usp.br

† berthha@usp.br

‡ jeferson@fisica.ufmt.br

§ alan@unifei.edu.br

¶ carlos.pellicer@ect.ufrn.br

## I. INTRODUCTION

Higher order terms in a field theory action including gravity are expected to appear in view of the high nonlinearity of gravity as well as due to corrections from string theories. Such higher order terms are rather unwanted, especially if there are higher order derivatives in the equations of motion, a case leading to a Hilbert space with a nonpositive scalar product. Even at a classical level higher derivative interactions are well known to lead to instabilities. However, Horndeski showed that there is a large class of fields which, in spite of having derivative terms of arbitrary order in the action, yield equations of motion at most second order in the derivatives [1], preventing, in principle, instabilities.

More recently, these ideas were used to describe a scalar fulfilling a second order equation of motion and which, moreover, obeyed a Galilean invariance [2, 3]. Cosmology also has several implications in the case of the presence of Horndeski scalars [4]. Problems related to instabilities are very important and Horndeski theories offer a good example of such phenomena [5]. The most important new term in the action is the coupling of the scalar field derivative with the Einstein curvature tensor  $G_{\mu\nu}$ , the so-called derivative coupling term,

$$\delta\mathcal{L} = \bar{z}\sqrt{-g}G^{\mu\nu}\partial_\mu\phi\partial_\nu\phi \quad . \quad (1)$$

The new interaction term behaves as a friction term for  $\bar{z} > 0$  in cosmological contexts, while a negative sign may lead to instability. Moreover, the derivative coupling term has been used in other physical contexts with interesting results, such as new solutions and nonperturbative effects [6–12], quasinormal modes [13, 14], structure formation [15], self-accelerating solutions [2], and disformal transformations in the dark sector [16]. Such a term also represents a drag or a boost to the fields, depending on the sign; thus, it can be of importance to the AdS/CFT conjecture as a means of a possible source of new physics, since the coupling to the Einstein tensor can be related to impurities in a superconductor [17].

Our primary aim is to consider the effects of such a term on the stability of a specific black hole solution. The probe fields we will consider are vectors and spinors obeying Maxwell/Proca and Dirac equations, respectively. As most studies of quasinormal modes around black holes focus on scalar fields due to their applications in cosmology, our motivation here is to use other fields with richer structure and more degrees of freedom that can reveal new features of the background model. In the following sections, we describe the

Galileon black hole metric considered here, set the corresponding perturbation equations, and compute as well as analyze the quasinormal spectrum using numerical methods.

## II. GALILEON BLACK HOLE SOLUTIONS

We consider a model described by an action consisting of the Einstein-Hilbert term plus a scalar field kinetically coupled to the curvature given by

$$S = \frac{1}{2} \int d^4x \sqrt{-g} [\beta R - (g^{\mu\nu} - \bar{z} G^{\mu\nu}) \partial_\mu \phi \partial_\nu \phi], \quad (2)$$

where  $\beta = m_p^2$ ,  $\bar{z} = \frac{z}{m_p^2}$  and  $G^{\mu\nu}$  is the Einstein tensor. The presence of this nonminimal derivative coupling has far-reaching consequences. One of the most important is the fact that if it plays the role of dark energy the speed of propagation of gravitational waves get corrections that may be easily detected but have not been until present times [18, 19], which has a negative impact on its uses for cosmology<sup>1</sup>. However, in view of the potential ubiquity of derivative terms in string inspired cosmology, Horndeski theories remain important as a realistic possibility, and the understanding of its role (and possible outcome of the above failure) is worth considering, at least for very high energies.

Since there is no scalar potential, the action is invariant under shift symmetry  $\phi \rightarrow \phi + const$ . This is precisely the reason to name  $\phi$  a Galileon field. Moreover, the  $\bar{z}$  term plays the role of the friction term alluded to above.

Varying the action with respect to the metric, we obtain the corresponding field equation,

$$\begin{aligned} & \beta \left( \frac{1}{2} g^{\lambda\kappa} R - R^{\lambda\kappa} \right) + \frac{1}{2} \partial^\nu \phi \partial_\nu \phi g^{\lambda\kappa} - \partial^\lambda \phi \partial^\kappa \phi + \bar{z} \left[ \frac{1}{2} R^{\mu\nu} \partial_\mu \phi \partial_\nu \phi g^{\lambda\kappa} - 2 R^{\mu\kappa} \partial_\mu \phi \partial^\lambda \phi + \frac{1}{2} R \partial^\lambda \phi \partial^\kappa \phi \right. \\ & \left. + \frac{1}{2} \left( R^{\lambda\kappa} - \frac{1}{2} g^{\lambda\kappa} R \right) \partial^\nu \phi \partial_\nu \phi - \partial^\lambda \partial^\kappa \phi \square \phi - \frac{1}{2} \partial_\alpha \partial_\nu \phi \partial^\alpha \partial^\nu \phi g^{\lambda\kappa} + \partial^\lambda \partial_\nu \phi \partial^\kappa \partial^\nu \phi + \frac{1}{2} (\square \phi)^2 g^{\lambda\kappa} \right] = 0. \end{aligned} \quad (3)$$

Furthermore, varying Eq.(2) with respect to  $\phi$ , we obtain the Galileon field equation,

$$\partial_\mu [\sqrt{-g} (\partial^\mu \phi - 2\bar{z} G^{\mu\nu} \partial_\nu \phi)] = 0. \quad (4)$$

In the spirit of Refs. [20, 21] black hole solutions for  $z > 0$  (for the case  $z < 0$  see comment

---

<sup>1</sup> Nonetheless, with some combinations of Horndeski Lagrangians it is still possible to obtain  $c_{gw} \approx c$  provided that their effects are negligible at late times [19]

<sup>2</sup>), as those ([6, 7]) can be obtained in the standard way from (3) and (4). With the ansatz

$$ds^2 = -F(r)dt^2 + H(r)dr^2 + r^2(d\theta^2 + \sin^2\theta d\phi^2), \quad (5)$$

one finds, as a result,

$$F(r) = \frac{3}{4} + \frac{r^2}{L^2} - \frac{2M}{m_P^2 r} + \frac{\sqrt{\bar{z}}}{4r} \arctan\left(\frac{r}{\sqrt{\bar{z}}}\right), \quad (6)$$

$$H(r) = \frac{(r^2 + 2\bar{z})^2}{4(r^2 + \bar{z})^2 F(r)}, \quad (7)$$

$$[\phi'(r)]^2 = -\frac{m_P^2 r^2 (r^2 + 2\bar{z})^2}{4\bar{z}(r^2 + \bar{z})^3 F(r)}, \quad (8)$$

where  $L^2 = 12\bar{z}$  and  $M$  is an integration constant related to the black hole mass. We notice that  $\bar{z}$  behaves as a nonperturbative parameter that interpolates between the Schwarzschild solution (for  $z \rightarrow \infty$ ) and Schwarzschild anti-de Sitter (AdS) solution. Out of these limits the Galileon black hole geometry is asymptotically AdS, which makes it interesting in the context of AdS/CFT correspondence.

A thermodynamical analysis of these solutions shows that large mass or small  $z$  parameter black holes are thermodynamically stable, while small mass black holes or alternatively having a large  $z$  parameter undergo a phase transition to the vacuum solution [6]. As a thermodynamical stability or instability does not imply a dynamical one *a priori*, we are interested in studying the evolution of matter fields in these black hole backgrounds with the aim of testing not only its stability but also to understand their interpretation in the case of AdS/CFT correspondence.

### III. VECTOR FIELD PERTURBATIONS

Electromagnetic perturbations are important in the context of the AdS/CFT conjecture since they can be related to perturbations of generic supergravity gauge fields. Moreover, Maxwell and Proca fields have unique features, possibly with an impact on tera-electron-volt scale gravity scenarios [22, 23]. In addition, higher order couplings including gauge fields have several new implications in the dynamics of gravity and spacetime; see Refs. [24] for discussions on this point.

---

<sup>2</sup> In the case  $z < 0$  the solution tends to a dS space. However, the metric turns out to be non-differentiable and a non-trivial stress-energy tensor needs to be added to the Lagrangian.

## A. Maxwell field

The evolution of the electromagnetic perturbation is given by the Maxwell equations without source,

$$\nabla_\nu F^{\nu\mu} = 0, \quad (9)$$

where the Maxwell tensor is given by

$$F_{\mu\nu} = \partial_\mu A_\nu - \partial_\nu A_\mu \quad (10)$$

The vector potential can be decomposed in components with odd (axial) and even (polar) parity as

$$A_\mu(t, r, \theta, \phi) = \sum_{\ell, m} \left( \begin{bmatrix} 0 \\ 0 \\ \frac{a(r, t)}{\sin\theta} \frac{\partial Y}{\partial\phi} \\ -a(r, t) \sin\theta \frac{\partial Y}{\partial\theta} \end{bmatrix} + \begin{bmatrix} f(r, t)Y \\ j(r, t)Y \\ k(r, t) \frac{\partial Y}{\partial\theta} \\ k(r, t) \frac{\partial Y}{\partial\phi} \end{bmatrix} \right). \quad (11)$$

Substituting back into Maxwell equations (9) we obtain the equation of motion

$$-\frac{\partial^2 \Psi(r, t)}{\partial t^2} + \frac{\partial^2 \Psi(r, t)}{\partial r_*^2} - V_M(r) \Psi(r, t) = 0, \quad (12)$$

where the tortoise coordinate is given by

$$dr_* = \sqrt{\frac{H(r)}{F(r)}} dr, \quad (13)$$

and the wave function  $\Psi(r, t)$  is a linear combination of  $a(r, t)$ ,  $f(r, t)$ ,  $j(r, t)$ , and  $k(r, t)$  as follows

$$\Psi^{axial}(r, t) = a(r, t), \quad \Psi^{polar}(r, t) = \frac{r^2 [j(r, t)_{,t} - f(r, t)_{,r}]}{\sqrt{F(r)H(r)} \ell(\ell + 1)}. \quad (14)$$

In both cases the effective potential can be written as

$$V_M(r) = F(r) \frac{\ell(\ell + 1)}{r^2}. \quad (15)$$

Inspecting Eqs.(12) and (15) one can see that the electromagnetic perturbations have a simplifying symmetry obtained by rescaling the spacetime variables  $t = \tau\sqrt{\bar{z}}$  and  $r = x\sqrt{\bar{z}}$  and the black hole mass as  $M = M'\sqrt{\bar{z}}$ . Such a result can be explicitly checked in the corresponding tables shown in the Appendix. In the spatial infinity, the electromagnetic

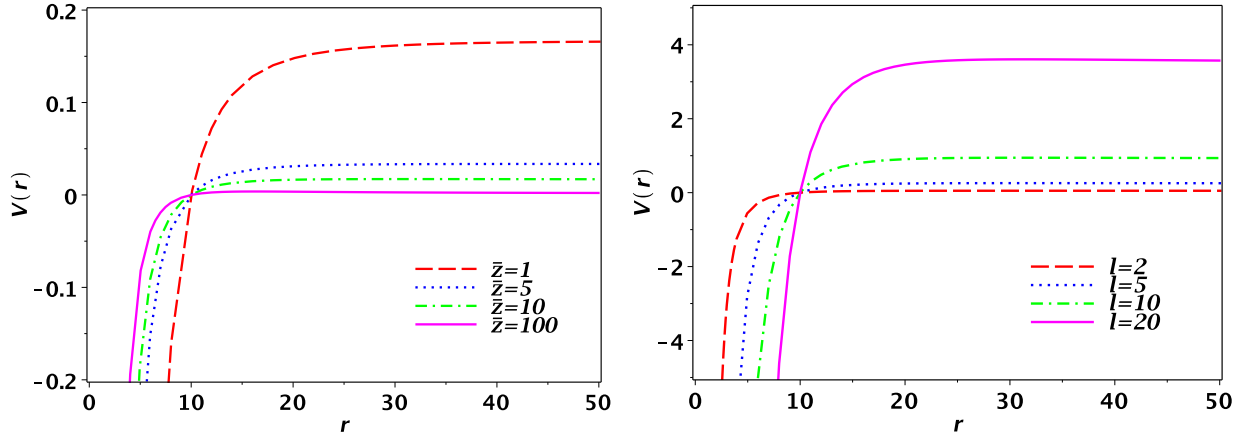


FIG. 1. Effective potential as a function of  $r$  for Maxwell perturbations fixing the event horizon at  $r_+ = 10$  for several values of  $\bar{z}$  fixing  $\ell = 1$  (left) and several values of  $\ell$  fixing  $\bar{z} = 10$ .

effective potential goes to a constant depending on  $\bar{z}$  and  $\ell$  as

$$V_M(r) \sim \frac{\ell(\ell + 1)}{12\bar{z}}. \quad (16)$$

Moreover,  $\Psi$  becomes independent of  $\bar{z}$ ,

$$\Psi(r) = C_1 + \frac{C_2}{r}. \quad (17)$$

We plotted the Maxwell potential (15) as a function of  $r$  in Fig.1. We can see that as  $\bar{z}$  increases for fixed multipole number  $\ell$  the asymptotic value becomes lower. The inverse effect is produced by increasing  $\ell$  for fixed  $\bar{z}$ . These results are in perfect agreement with Eq.(16).

## B. Proca field

Now, we consider massive electromagnetic perturbations, which can be modeled using Proca field equations given by

$$\nabla_\nu F^{\nu\mu} - m^2 A^\mu = 0 \quad , \quad (18)$$

where  $m$  is the mass of the Proca field. The above equation can be decomposed in odd (axial) and even (polar) components as in (11). The equation of motion for the axial component of

the vector field turns out to be

$$-\frac{\partial^2 \Psi_P^{axial}}{\partial t^2} + \frac{\partial^2 \Psi_P^{axial}}{\partial r_*^2} - V_P^{axial}(r) \Psi_P^{axial} = 0, \quad (19)$$

where again  $\Psi_P^{axial}(r, t)$  is shown in (14), the tortoise coordinate is given by (13), and the effective potential  $V_P^{axial}$  reads

$$V_P^{axial}(r) = F(r) \left[ \frac{\ell(\ell+1)}{r^2} + m^2 \right]. \quad (20)$$

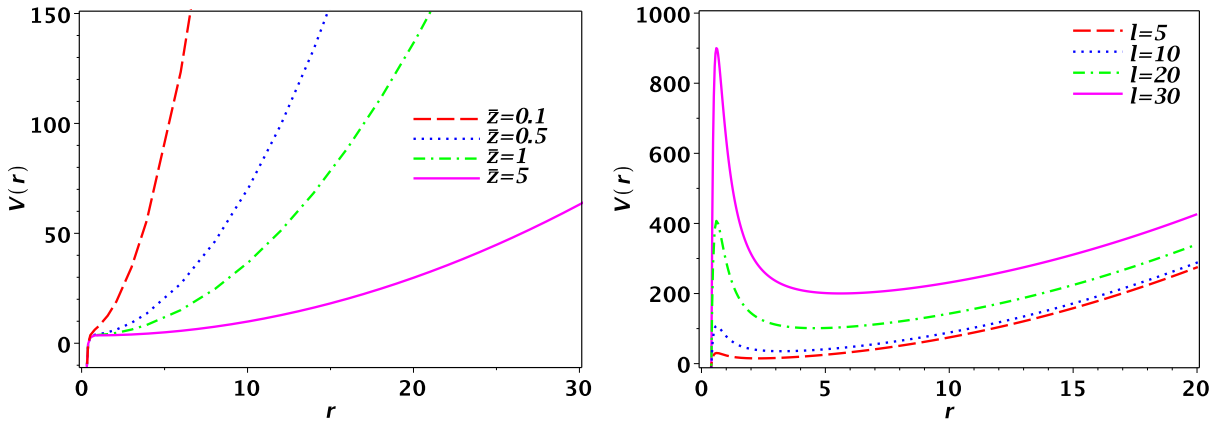


FIG. 2. Effective potential as a function of  $r$  for axial Proca perturbations for  $m = 2$ , fixing  $\ell = 1$  for several values of  $\bar{z}$  (left) and fixing  $\bar{z} = 0.5$  for several values of  $\ell$  (right). The event horizon is located at  $r_+ = 0.4$ .

Figure 2 shows the effective potential as a function of  $r$  for axial Proca perturbations. From Eq.(20) it is easy to see that for large  $r$  the mass term dominates, so the potential diverges as  $r^2$ , a fact that can also be noticed from the plots. For large multipole number the potential develops a peak near the event horizon, but it remains always positive definite.

The polar component can be arranged in a set of coupled equations of motion given by

$$\frac{F(r)}{\sqrt{F(r)H(r)}} \left[ \frac{[j(r, t),_t - f(r, t),_r] r^2}{\sqrt{F(r)H(r)}} \right]_{,r} = [k(r, t),_t - f(r, t)] \ell(\ell+1) - m^2 r^2 f(r, t), \quad (21)$$

$$\frac{H(r)}{\sqrt{F(r)H(r)}} \left[ \frac{[j(r, t),_t - f(r, t),_r] r^2}{\sqrt{F(r)H(r)}} \right]_{,t} = [k(r, t),_r - j(r, t)] \ell(\ell+1) - m^2 r^2 j(r, t). \quad (22)$$

Equations (21) and (22) cannot be decoupled for arbitrary values of multipoles  $\ell$ . However, for the monopole mode ( $\ell = 0$ ), these equations become decoupled. In fact, this case

corresponds to a scalar mode. Although this is forbidden for the Maxwell field, which has only two helicities, it is certainly possible for the Proca field (due to its mass). Thus, rewriting Eqs. (21) and (22) and performing a substitution in terms of a new function  $N(r, t)$ , we have

$$\frac{F(r)}{\sqrt{F(r)H(r)}}[N(r, t)r^2]_{,r} = -m^2r^2f(r, t), \quad (23)$$

$$\frac{H(r)}{\sqrt{F(r)H(r)}}[N(r, t)r^2]_{,t} = -m^2r^2j(r, t), \quad (24)$$

where the function  $N(r, t)$  is defined by

$$N(r, t) = \frac{[j(r, t)_{,t} - f(r, t)_{,r}]}{\sqrt{F(r)H(r)}}. \quad (25)$$

Deriving Eq.(23) with respect to  $r$  and Eq.(24) with respect to  $t$  and adding the resulting equations we obtain

$$-\frac{\partial^2 N(r, t)}{\partial t^2} + \frac{\partial^2 N(r, t)}{\partial r_*^2} + \frac{\partial}{\partial r_*} \left[ \frac{2}{r} \sqrt{\frac{F}{H}} N(r, t) \right] - m^2 F N(r, t) = 0. \quad (26)$$

Setting  $N(r, t) = \frac{R(r, t)}{r}$ , Eq.(26) turns out to be

$$-\frac{\partial^2 R(r, t)}{\partial t^2} + \frac{\partial^2 R(r, t)}{\partial r_*^2} - V_P^{polar}(r)R(r, t) = 0, \quad (27)$$

with the effective potential expressed as

$$V_P^{polar}(r) = \left[ \frac{2}{r^2} \frac{F}{H} + m^2 F - \frac{1}{2r} \left( \frac{F}{H} \right)_{,r} \right]. \quad (28)$$

Figure 3 shows the effective potential as a function of  $r$  for polar Proca perturbations. As we can observe,  $\bar{z}$  and  $m$  have similar effects on the form of the potential. When one of them is fixed, and the other parameter modifies the depth and width of the negative potential well near the event horizon. In fact, the smaller this varying parameter is, the deeper and wider the well becomes. Another interesting feature is that there is a range of values from 0 to  $m_*$  or  $\bar{z}_*$  for which the well appears right outside the event horizon. When  $m > m_*$  or  $\bar{z} > \bar{z}_*$ , the well is shifted to values  $r < r_+$ , so it is not relevant for our study anymore. Furthermore, as  $m$  increases, the potential diverges as  $r^2$  in a faster manner.

A redefinition of the mass in the potentials presented in Eqs.(20) and (28) as  $m^2 = \mu^2/\bar{z}$  makes both, axial and polar massive electromagnetic perturbations, invariant by the same coordinate transformation previously discussed.



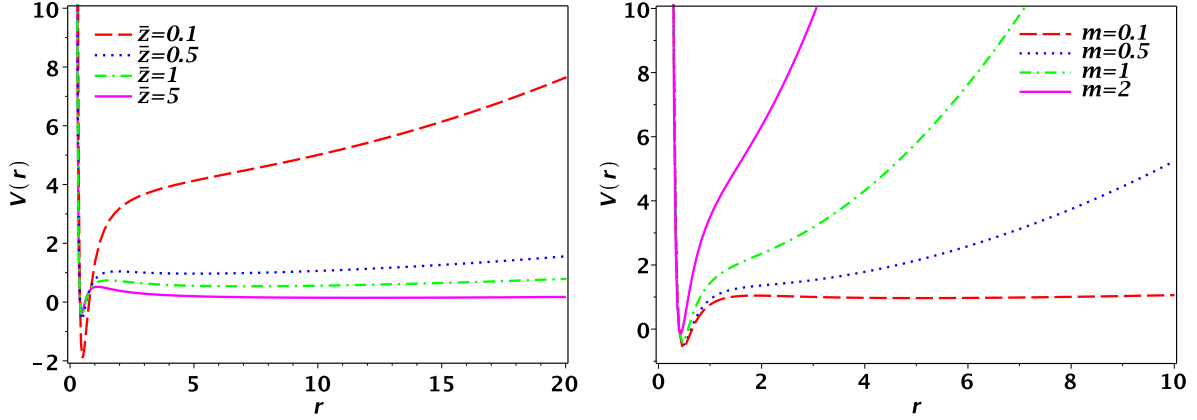


FIG. 3. Effective potential as a function of  $r$  for polar Proca perturbations fixing  $m = 0.1$  for several values of  $\bar{z}$  (left) and fixing  $\bar{z} = 0.5$  for several values of Proca field mass  $m$  (right). The event horizon is located at  $r_+ = 0.4$ .

In the spatial infinity ( $r \rightarrow \infty$ ), axial and polar Proca effective potentials reduce to the same value

$$V_P(r) \sim \frac{m^2 r^2}{12\bar{z}}, \quad (29)$$

which is consistent with the graph analysis. Also, different from the Maxwell case, both components of the Proca field  $\Psi$  will become

$$\Psi(r) = \frac{C_1}{r^{\alpha_+}} + \frac{C_2}{r^{\alpha_-}}, \quad (30)$$

where

$$\alpha_{\pm} = \frac{1}{2} \pm \frac{\sqrt{1 + 9m^2\bar{z}}}{2}. \quad (31)$$

In this case we also obtain the above-mentioned symmetry for Maxwell perturbations by rescaling the spacetime variables  $t = \tau\sqrt{\bar{z}}$  and  $r = x\sqrt{\bar{z}}$  and the black hole mass as  $M = M'\sqrt{\bar{z}}$ , such that (for a given Proca mass) the quasinormal mode frequency scales as

$$\omega = \frac{1}{\sqrt{\bar{z}}} \mathbf{f} \left( \frac{r_+}{\sqrt{\bar{z}}} \right), \quad (32)$$

where  $\mathbf{f}$  is a real function. Such a result can explicitly be checked in the corresponding tables shown in the Appendix.

#### IV. FERMIONIC FIELD PERTURBATION

One of the most interesting possibilities is the introduction of fermions in the model. Let us consider a spinorial field  $\Psi$  with mass  $\mu_s$  as a perturbation in the spacetime given by Eq.(5), obeying Dirac equation,

$$i\gamma^{(a)}e_{(a)}^\mu\nabla_\mu\Psi - \mu_s\Psi = 0, \quad (33)$$

where the covariant derivative is defined according to

$$\nabla_\mu = \partial_\mu + \frac{1}{4}\omega_\mu^{(a)(b)}\gamma_{[a}\gamma_{b]}, \quad (34)$$

and  $\omega_\mu^{(a)(b)}$  is the spin connection written in terms of the tetrad basis  $e_\mu^{(a)}$  as

$$\omega_\mu^{(a)(b)} = e_\nu^{(a)}\partial_\mu e^{(b)\nu} + e_\nu^{(a)}\Gamma_{\mu\sigma}^\nu e^{\sigma(b)}. \quad (35)$$

Here greek indices refer to spacetime coordinates  $(t, r, \theta, \phi)$ , while latin indices enclosed in parentheses are assigned to flat tangent space where the tetrad basis is defined. The Dirac matrices  $\gamma^{(a)}$  are given by

$$\gamma^0 = \begin{pmatrix} -i & 0 \\ 0 & i \end{pmatrix}, \quad \gamma^i = \begin{pmatrix} 0 & -i\sigma^i \\ i\sigma^i & 0 \end{pmatrix}, \quad i = 1, 2, 3, \quad (36)$$

where  $\sigma^i$  are the Pauli matrices. Using metric (5) we can specify the tetrad basis as

$$e_0^{(a)} = \sqrt{F}\delta_0^{(a)}, \quad e_1^{(a)} = \sqrt{G}\delta_1^{(a)}, \quad e_2^{(a)} = r\delta_2^{(a)}, \quad e_3^{(a)} = r\sin\theta\delta_3^{(a)}. \quad (37)$$

Thus, the Dirac equation (33) becomes

$$\left[ \gamma^0 \left( \frac{1}{\sqrt{F}} \right) \partial_t + \gamma^1 \left( \frac{1}{\sqrt{H}} \right) \left( \partial_r + \frac{1}{4} \frac{F'}{F} + \frac{1}{r} \right) + \gamma^2 \left( \frac{1}{r} \right) \left( \partial_\theta + \frac{1}{2} \cot \theta \right) + \gamma^3 \left( \frac{1}{r \sin \theta} \right) \partial_\phi + i\mu_s \right] \Psi = 0.$$

In order to simplify this equation, let us define

$$\Psi(t, r, \theta, \phi) = F(r)^{-1/4} \Phi(t, r, \theta, \phi); \quad (38)$$

thus, Eq.(38) becomes

$$\left[ \gamma^0 \left( \frac{1}{\sqrt{F}} \right) \partial_t + \gamma^1 \left( \frac{1}{\sqrt{H}} \right) \left( \partial_r + \frac{1}{r} \right) + \gamma^2 \left( \frac{1}{r} \right) \left( \partial_\theta + \frac{1}{2} \cot \theta \right) + \gamma^3 \left( \frac{1}{r \sin \theta} \right) \partial_\phi + i\mu_s \right] \Phi = 0. \quad (39)$$

Notice that when  $F(r) = H(r)^{-1} = (1 - 2M/r)$  Eq.(39) reduces to the Schwarzschild case [25].

By decomposing Dirac equation in an angular and a two-dimensional  $(t, r)$  part [26], for a two-spinor the latter equation reads

$$\left( \partial_t - \sqrt{\frac{F}{H}} \partial_r \right) \psi_2 = \left( i\kappa \frac{\sqrt{F}}{r} + i\mu_s \sqrt{F} \right) \psi_1 \quad (40)$$

$$\left( \partial_t + \sqrt{\frac{F}{H}} \partial_r \right) \psi_1 = - \left( i\kappa \frac{\sqrt{F}}{r} + i\mu_s \sqrt{F} \right) \psi_2, \quad (41)$$

where  $\kappa$  is a constant associated to the variable separation that can be expressed as  $\kappa = i(\ell + 1) \equiv iK$ . By writing the two-spinor components as

$$\psi_1 = e^{-i\omega t} R_1(r) \quad (42)$$

$$\psi_2 = e^{-i\omega t} R_2(r), \quad (43)$$

and switching to the tortoise coordinate (13), Eqs.(40) and (41) become

$$\left( \frac{d}{dr_*} + i\omega \right) R_2 = \sqrt{F} \left( \frac{K}{r} + i\mu_s \right) R_1 \quad (44)$$

$$\left( \frac{d}{dr_*} - i\omega \right) R_1 = \sqrt{F} \left( \frac{K}{r} - i\mu_s \right) R_2. \quad (45)$$

Now, we define a new function  $\theta$ , set a new tortoise coordinate  $\hat{r}_*$ , and rescale again the spinorial components  $R_1$  and  $R_2$  through the expressions

$$\theta = \arctan \left( \frac{\mu_s r}{K} \right), \quad \hat{r}_* = r_* + \frac{1}{2\omega} \arctan \left( \frac{\mu_s r}{K} \right), \quad (46)$$

$$R_1 = e^{-i\theta/2} \Phi_1 \text{ and } R_2 = e^{i\theta/2} \Phi_2. \quad (47)$$

Thus, Eqs.(44) and (45) turn out to be

$$\left( \frac{d}{d\hat{r}_*} \pm i\omega \right) \Phi_{(2)} = W \Phi_{(1)}, \quad (48)$$

where the so-called superpotential can be written as

$$W = \frac{[F(K^2/r^2 + \mu_s^2)]^{1/2}}{1 + \frac{\mu_s K}{2\omega(K^2 + \mu_s^2 r^2)} \sqrt{\frac{F}{H}}}. \quad (49)$$

Finally, in order to express our result in a more familiar way in terms of the superpartner potentials, let us define

$$Z_{\pm} = \Phi_1 \pm \Phi_2. \quad (50)$$

Thus, Eqs.(48) can be brought to their final form,

$$\left(\frac{d^2}{d\hat{r}_*^2} + \omega^2\right) Z_{\pm} = V_{\pm} Z_{\pm}, \quad (51)$$

with the superpartner potentials given by

$$V_{\pm} = W^2 \pm \frac{dW}{d\hat{r}_*}. \quad (52)$$

In what follows, we will consider the case of a massless fermion field. In this case the superpotential (49) reduces to

$$W = \sqrt{F} \frac{K}{r}. \quad (53)$$

The superpartner potentials  $V_+$  and  $V_-$  yield the same quasinormal spectrum since they satisfy the relation

$$V_+ - V_- - 2\frac{dW}{dr_*} = 0. \quad (54)$$

Notice that both tortoise coordinates coincide when  $\mu_s = 0$ .

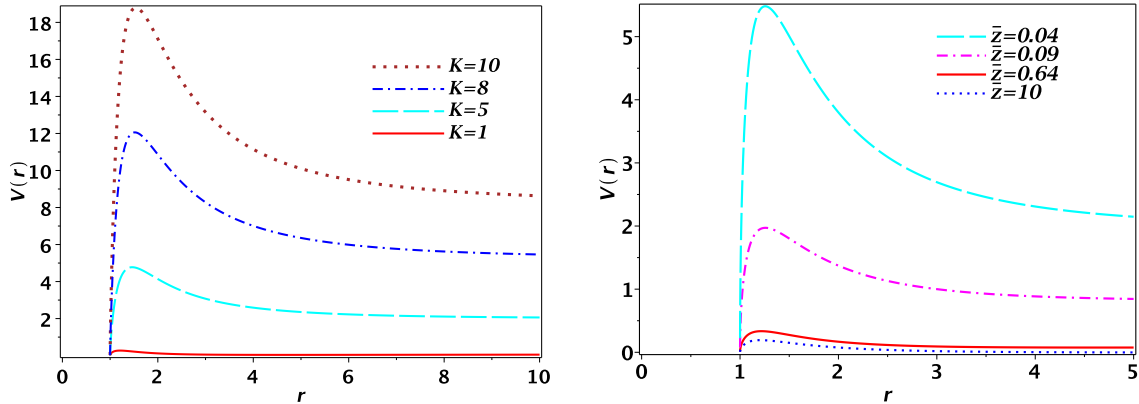


FIG. 4. Effective potential  $V_+$  as a function of  $r$  for spinorial perturbations fixing  $\bar{z} = 1$  for different  $K$  (left) and fixing  $K = 1$  for different  $\bar{z}$  (right). Notice that event the horizon is located at  $r_+ = 1$ .

From Figs. 4 and 5, we see that superpartner effective potentials display a maximum (or minimum in the case of  $V_-$  for small  $\bar{z}$ ) around the event horizon neighborhood and decrease to a constant value as the radial coordinate goes to infinity,

$$\lim_{r \rightarrow \infty} V_+ = \lim_{r \rightarrow \infty} V_- \rightarrow \frac{K^2}{12\bar{z}}. \quad (55)$$

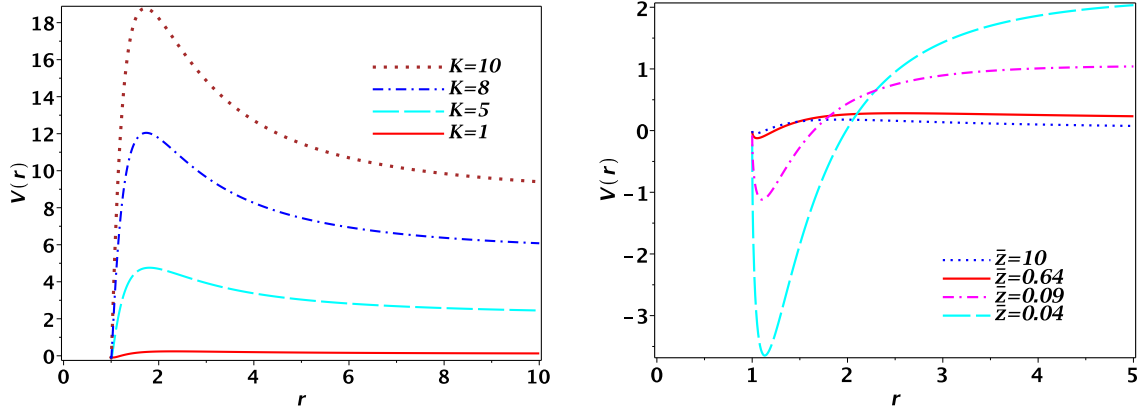


FIG. 5. Effective potential  $V_-$  as a function of  $r$  for spinorial perturbations fixing  $\bar{z} = 1$  for different  $K$  (left) and fixing  $K = 1$  for different  $\bar{z}$  (right). Notice that the event horizon is located at  $r_+ = 1$ .

For both potentials, as  $K$  grows, a peak rises up. On the other hand, as the  $\bar{z}$  parameter increases, the peak in  $V_+$  or the well in  $V_-$  decreases and gradually reaches the curves corresponding to nonmassive fermions propagating in a Schwarzschild solution. This result perfectly agrees with the fact that metric (5) approaches the Schwarzschild solution in the limit  $\bar{z} \rightarrow \infty$ .

From this behavior it is clear that we can apply a WKB method to obtain quasinormal frequencies. It is well known that the WKB method has a perfect convergence when the parameter associated to the angular momentum is large compared to the overtone number. In other cases we must analyze other parameters to reach some conclusion.

Looking at Fig. 5, it is clear that the potential  $V_-$  is a very curious case. As  $\bar{z}$  becomes smaller, a negative well develops and some instabilities could be expected. However, no instability was found in our numerical calculation. In order to explain this fact, we approximated the region near the  $V_-$  minimum as a harmonic oscillator potential and found the ground state energy of the associated state. Performing this procedure numerically, we discovered that this energy is always larger than the depth of the well. Thus, we have no bound states, and no unstable mode can exist.

## V. NUMERICAL RESULTS

### A. Massless vector field

Let us begin our discussion by showing the results for Maxwell perturbations.

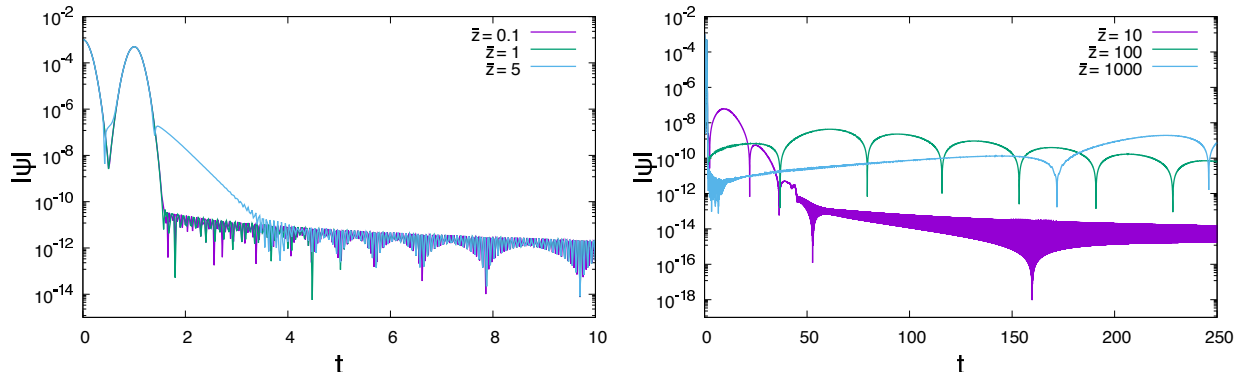


FIG. 6. Maxwell perturbations for different values of  $\bar{z}$  with multipole number  $\ell = 1$  and the event horizon fixed at  $r_+ = 100$  (left) and  $r_+ = 10$  (right).

In Fig.6, we show some of our results for small and big values of  $\bar{z}$  compared to the event horizon with multipole number  $\ell = 1$ . From these figures we can see that for small values of  $\bar{z}$  modes appear to be stable and display oscillating tails. Although these perturbations are massless, these tails are a strong indication that  $\bar{z}$  plays the role of mass for the perturbation. We can also notice that when  $\bar{z}$  gets bigger, the imaginary part of the frequencies decreases but it does not reach zero. We also verified that for bigger multipole numbers  $\ell$  modes with  $\bar{z}$  of the order of the event horizon produce beats and the oscillating tails decay more slowly. Thus, we can conclude that the model is stable under Maxwell perturbations.

We also used the Horowitz-Hubeny (HH) method [27] in order to numerically obtain the quasinormal frequencies. Our results are shown in Tables I and II in the Appendix. For small black holes ( $r_+ < 1$ ) when  $\bar{z} > r_+$  the task of finding quasinormal frequencies becomes harder and the convergence of the HH method becomes worse. We can see that a critical value of  $\bar{z}_{cI}$ , indicated with a \* in the tables, satisfies the following relation  $\bar{z}_{cI} \sim 0.0178 r_+^2$ . For  $\bar{z} < \bar{z}_{cI}$  quasinormal modes become purely imaginary like in a damped harmonic oscillator.

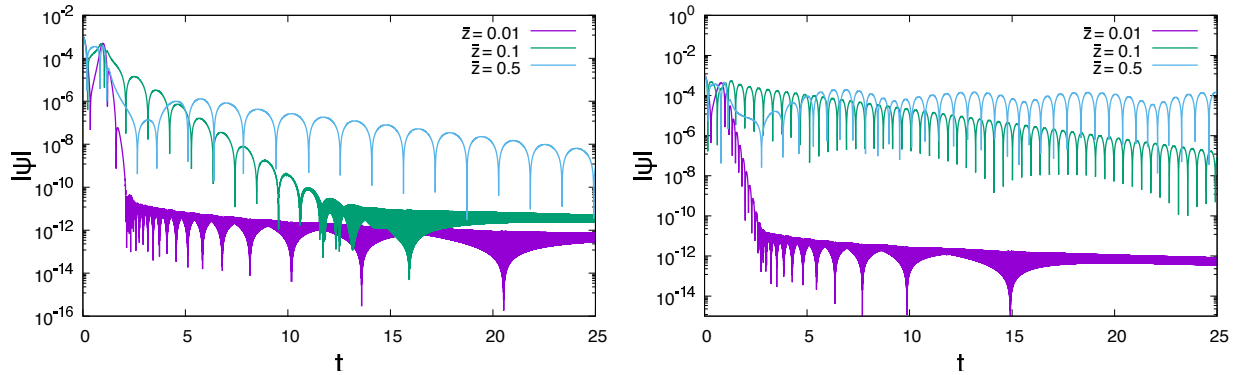


FIG. 7. Axial Proca perturbations for  $m = 2$  when  $\ell = 1$  (left) and  $\ell = 5$  (right) for different values of  $\bar{z}$ . In both cases we set the event horizon at  $r_+ = 0.4$ .

## B. Massive vector field

Now let us turn our attention to Proca perturbations. In Fig.7, we show our results for axial Proca perturbations fixing the vector field mass  $m = 2$  for several values of  $\bar{z}$ .

Our results establish that modes with small multipole number  $\ell$  are always decaying pointing out the stability of the model under this kind of perturbation. For given values of  $r_+$ ,  $m$  and  $\ell$ , as  $\bar{z}$  grows, the modes decay in a slower manner and some of them present oscillating beats and oscillating tails. Also, as we can infer from Eq.(20), if  $m$  increases, the modes are damped more rapidly as the potential is dominated by the  $m$  term.

When we consider larger multipole numbers  $\ell$  and  $\bar{z}$  around the same order of the event horizon, long-living nondamped oscillating modes, the so-called quasinormal modes (QRM) [28–30], begin to appear. This can be understood by looking at the corresponding potential shape in Fig.2. As  $\ell$  grows, a positive well appears in the potential making possible the appearance of modes which are trapped inside the well and begin to oscillate with real frequency.

Table III in the Appendix shows the quasinormal frequencies obtained by the HH method. As mentioned in previous sections, we can clearly see a symmetry by rescaling the spacetime variables as well as the black hole mass, such that the frequencies fulfill Eq.(32).

In the case of polar Proca modes we can see the evolution of the perturbations in Fig.8. We can observe that for small field mass  $m$  perturbations decay more slowly than for bigger

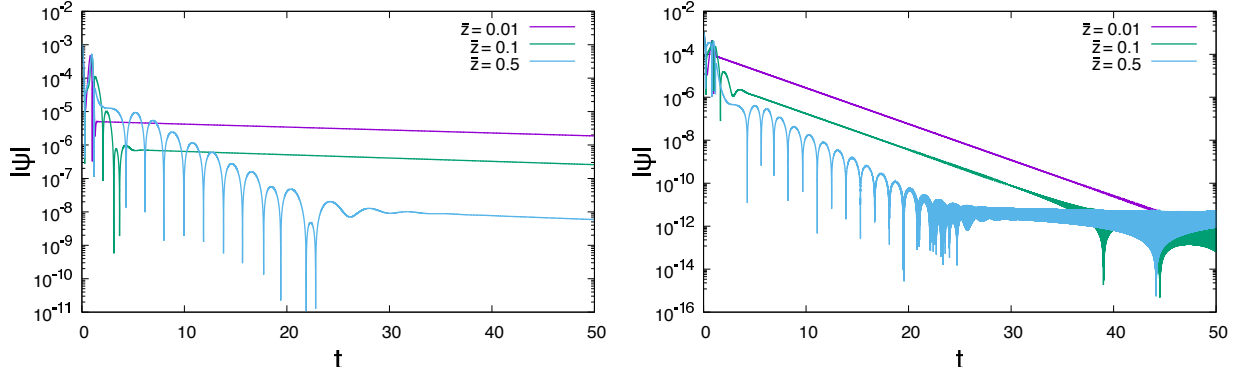


FIG. 8. Polar Proca perturbations for  $m = 0.1$  (left) and  $m = 2$  (right) for different values of  $\bar{z}$ . In both cases, we set the event horizon at  $r_+ = 0.4$ .

mass. In addition, for small values of  $\bar{z}$  compared to the event horizon we can check that after a fast decay there is a power-law tail. And when  $\bar{z}$  gets of the same order of the event horizon, oscillating beats appear. Thus, the model is stable under this kind of perturbation.

In Table IV in the Appendix our results using the HH method are displayed. Again, there is a critical value  $\bar{z}_{cI}$  below which the modes become purely imaginary.

### C. Massless spinorial field and Klein paradox

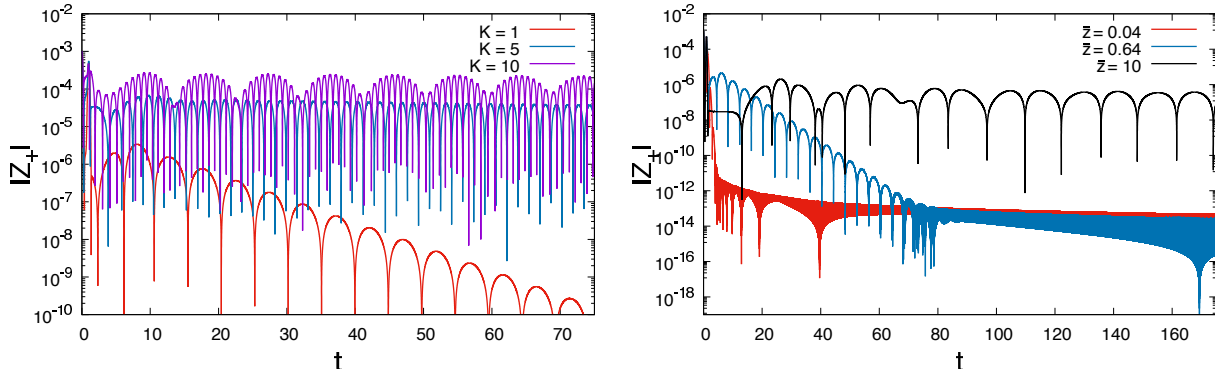


FIG. 9. Spinorial perturbations for superpartner potential  $V_+$  for different values of  $K$  fixing  $\bar{z} = 1$  (left) and for different values of  $\bar{z}$  fixing  $K = 1$  (right). In both cases we set the event horizon at  $r_+ = 1$ .



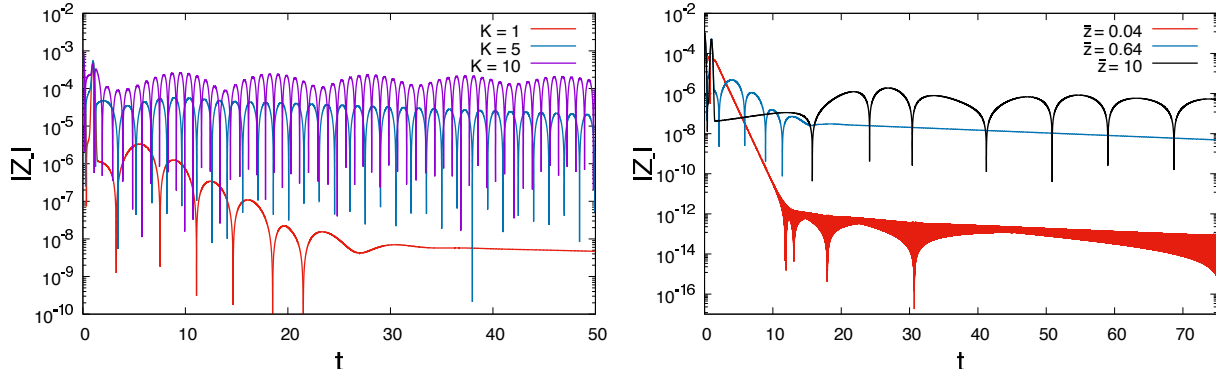


FIG. 10. Spinorial perturbations for superpartner potential  $V_-$  for different values of  $K$  fixing  $\bar{z} = 1$  (left) and for different values of  $\bar{z}$  fixing  $K = 1$  (right). In both cases we set the event horizon at  $r_+ = 1$ .

Our results for quasinormal modes are displayed in Fig.9 for the superpartner potential  $V_+$  and Fig.10 for the superpartner potential  $V_-$ . They show that the model is stable for both  $\bar{z}/r_+ \lesssim 1$  and large  $\bar{z}$ . In particular, notice that we did not find any unstable mode for the Schwarzschild case, which agrees with the result shown in Ref. [25]. As  $\bar{z}$  grows, the imaginary part of the frequency gets smaller, but is still negative, so the modes decay more slowly. Moreover, when  $\bar{z} \rightarrow \infty$ , i.e., in the Schwarzschild limit, perturbations always decay with an oscillating tail. Both effects the longer-living modes and the oscillating tails have been related to the mass of the perturbation in other models (see Refs. [31–33] and references therein). Although we are dealing here with massless spinors, the responsible for both behaviors is the  $\bar{z}$  term that behaves like a mass term in the Lagrangian. Thus, our results perfectly agree with the well-known behavior in Schwarzschild spacetime, in which massive perturbations have oscillating tails.

Regarding the multipole number, when  $K$ , is small the perturbations decay more rapidly. One interesting feature displayed in Figs. 9 and 10 is the appearance of long-living non-damped oscillating modes, the so-called QRMs, for intermediate  $\bar{z}$  as  $K$  grows. We believe that these QRMs are related to the well-known Klein paradox. Originally, this paradox appears when studying an electron hitting a potential barrier [34–36]. According to non-relativistic quantum mechanics the electron can tunnel the barrier with a damped solution until a certain penetration distance. However, in relativistic quantum mechanics, the be-

havior is different and certainly odd. In fact, when the barrier's height reaches the mass of the electron  $V \sim m_e c^2$ , it becomes almost transparent to it. And even if the barrier becomes infinite the electron will always tunnel. In our case, it is easy to see from Figs. 4 and 5 that as  $K$  grows the barrier also grows so that at some point the massless Dirac mode considered here will borrow enough energy to tunnel and enter the region with constant potential where it behaves as a free particle. In Fig. 11, we show quasinormal frequencies for several values of  $\bar{z}$  and  $K$ . From these graphs, it is clear that QRMs naturally appear when  $\bar{z}$  is of the same order of  $r_+$ . This feature, however, could not be detected using WKB method, the results of which are shown in Table V in the Appendix. This is also clear in view of the semiclassical character of the WKB approximation, since the Klein paradox is a quantum effect. In our case small values of  $\sqrt{\bar{z}}$  compared to the event horizon, *i.e.*, far from the Schwarzschild solution, produce a poor WKB convergence. Nevertheless, we notice that convergence is much better for large multipole numbers where WKB and numerical methods produce similar real frequencies.

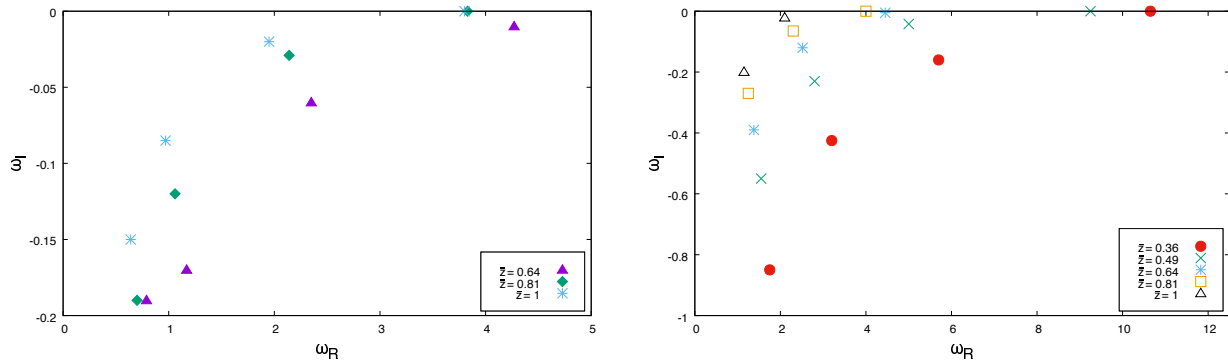


FIG. 11. Quasinormal frequencies for  $V_+$  (left) and  $V_-$  (right) for different values of  $\bar{z}$  as indicated in the legend. For each  $\bar{z}$ , there is a sequence of points, beginning from the smallest real frequency, that corresponds to a multipole number  $K = 1, 2, 5, 10$  for  $V_+$  and  $K = 2, 5, 10, 20$  for  $V_-$ .

## VI. CONCLUSIONS

We have considered perturbations on Galileon black holes obtained from Einstein gravity with a scalar field nonminimally coupled to Einstein tensor. Vector and fermionic pertur-

bations behave according to the expectations showing the stability of the model when the  $\bar{z}$  parameter is positive.

In the case of vector perturbations in both cases, Maxwell and Proca fields, there is a symmetry by rescaling the spacetime coordinates and the black hole mass such that quasinormal frequencies obey Eq.(32). This fact is also evident from the results produced by the HH method. In all cases we found no instability under these vector perturbations.

Regarding Dirac perturbation a new phenomenon, which is similar to Klein paradox arises; *i.e.*, a higher barrier in the potential implies a higher probability of long-living oscillating modes (QRMs) for intermediate values of the  $\bar{z}$  parameter and large multipole number  $K$ . This is a pure quantum phenomenon that we could only detect by numerically solving the corresponding Dirac equation. As WKB is a semiclassical approach, the quasinormal frequencies obtained in this way do not show this phenomenon. Again no instability under spinorial perturbations has been found so far.

The Galileon black hole model thus shows interesting effects that do not appear in a simple black hole, and new physics arises, providing new possible applications in the realm of the AdS/CFT framework. In cosmology a possible use can only be foreseen in very early phases of the Universe. Galileon scalar fields describing dark Energy are probably doomed by the effect of these fields in the speed of gravitational wave propagation, unless some new mechanism occurs.

## ACKNOWLEDGMENTS

This work was supported by CNPq (Conselho Nacional de Desenvolvimento Científico e Tecnológico), FAPESP (Fundação de Amparo à Pesquisa do Estado de São Paulo) and FAPEMIG (Fundação de Amparo à Pesquisa do Estado de Minas Gerais), Brazil.

## Appendix: Results of Horowitz-Hubeny and WKB Methods

- 
- [1] G. W. Horndeski, *Ont. J. Int. Phys.* **10**, 363 (1974).
  - [2] A. Nicolis, Riccardo Rattazzi, Enrico Trincherini *Phys. Rev.* **D79**, 064036 (2009).

TABLE I. Lowest massless vectorial (Maxwell field) quasinormal modes for a Rinaldi black hole with  $r_+ = 0.1$  (left) and  $r_+ = 1$  (right) produced using the HH method. The multipole number is  $\ell = 1$ . The \* signals the  $\bar{z}_{cI}$  critical value below which the modes are purely imaginary.

$\bar{z}$	$\omega_R$	$\omega_I$	$N$
0.00001	$\sim 0$	-2526.8773	40
0.00005	$\sim 0$	-528.8917	40
0.0001	$\sim 0$	-282.4976	40
0.000178*	$\sim 0$	-194.0150	40
0.0005	-27.9461	-67.3439	40
0.001	-21.7859	-32.5379	50
0.005	-11.0183	-5.5403	70
0.01	-8.3854	-2.2857	120
$\bar{z}$	$\omega_R$	$\omega_I$	$N$
0.001	$\sim 0$	-252.6877	30
0.005	$\sim 0$	-52.8892	30
0.01	$\sim 0$	-28.2498	30
0.0178*	$\sim 0$	-19.4015	35
0.05	-2.7946	-6.7344	40
0.1	-2.1786	-3.2538	60
0.5	-1.1018	-0.5540	70
1	-0.8384	-0.2286	130

[3] C. Deffayet, S. Deser, G. Esposito-Farese, *Phys. Rev.* **D80**, 064015 (2009).

[4] G. Koutsoumbas, K. Ntrekis, E. Papantonopoulos, E. N. Saridakis, *JCAP* **1802**, 003 (2018).

TABLE II. Lowest massless vectorial (Maxwell field) quasinormal modes for a Rinaldi black hole with  $r_+ = 10$  (left) and  $r_+ = 100$  (right) produced using the HH method. The multipole number is  $\ell = 1$ . The \* signals the  $\bar{z}_{cI}$  critical value below which the modes are purely imaginary.

$\bar{z}$	$\omega_R$	$\omega_I$	$N$	$\bar{z}$	$\omega_R$	$\omega_I$	$N$
0.1	$\sim 0$	-25.2688	40	1	$\sim 0$	-25.0265	30
0.5	$\sim 0$	-5.2889	40	10	$\sim 0$	-2.5269	30
1	$\sim 0$	-2.8250	40	50	$\sim 0$	-0.5289	40
1.78*	$\sim 0$	-1.9401	40	100	$\sim 0$	-0.2825	40
2	-0.1903	-1.7498	40	178*	$\sim 0$	-0.1940	35
5	-0.2795	-0.6734	40	180	-0.0055	-0.1952	35
10	-0.2179	-0.3254	60	200	-0.0190	-0.1750	50
50	-0.1102	-0.0554	70	500	-0.0279	-0.0673	50
150	-0.0719	-0.0126	180	1000	-0.0218	-0.0325	50

- [5] Th. Kolyvaris, M. Koukouvaou, A. Machattou, E. Papantonopoulos, *Phys. Rev.* **D98**, 024045 (2018).
- [6] M. Rinaldi, *Phys. Rev.* **D86**, 084048 (2012).
- [7] M. Minamitsuji, *Phys. Rev.* **D89**, 064017 (2014).
- [8] A. Anabalón, A. Cisterna and J. Oliva, *Phys. Rev. D* **89**, 084050 (2014).
- [9] A. Cisterna and C. Erices, *Phys. Rev. D* **89**, 084038 (2014).
- [10] A. Cisterna, T. Delsate and M. Rinaldi, *Phys. Rev. D* **92**, no. 4, 044050 (2015).
- [11] A. Cisterna, T. Delsate, L. Ducobu and M. Rinaldi, *Phys. Rev. D* **93**, no. 8, 084046 (2016).
- [12] Y. Brihaye, A. Cisterna and C. Erices, *Phys. Rev. D* **93**, no. 12, 124057 (2016).
- [13] M. Minamitsuji, *Gen. Rel. and Grav.* **46**, 1785 (2014).
- [14] R. A. Konoplya, Z. Stuchlík and A. Zhidenko, arXiv:1808.03346 [gr-qc].
- [15] E. Bellini, I. Sawicki, *JCAP* **1407** 050 (2014).
- [16] M. Zumalacarregui, T.S. Koivisto, D.F. Mota, P. Ruiz-Lapuente, *JCAP* **1005**, 038 (2010).
- [17] X-M. Kuang, E. Papantonopoulos, *JHEP* **1608**, 161 (2016).

- [18] LIGO Scientific and Virgo Collaborations, B. P. Abbott et al., *Phys. Rev. Lett.* **116** , 061102 (2016).
- [19] Y. Gong, E. Papantonopoulos, Z. Yi, arXiv:1711.04102.
- [20] L. Amendola, *Phys. Lett.* **B301**, 175 (1993).
- [21] S. V. Sushkov, *Phys. Rev.* **D80**, 103505 (2009).
- [22] E. Abdalla, B. Cuadros-Melgar, A. B. Pavan and C. Molina, *Nucl. Phys.* **B752**, 40 (2006).
- [23] N. Arkani-Hamed, S. Dimopoulos and G. Dvali, *Phys. Lett.* **429B** (1998) 263; *Phys. Rev.* **D59** 086004 (1999).
- [24] S. Chen, J. Jing *Phys. Rev.* **D90**, 124059 (2014).
- [25] H. T. Cho, *Phys. Rev.* **D68**, 024003 (2003).
- [26] A. López-Ortega, *Lat. Am. Jour. Phys. Educ.* **3**, 578 (2009).
- [27] G. T. Horowitz and V. E. Hubeny, *Phys. Rev.* **D62**, 044009 (2002).
- [28] A. Ohashi, M. Sakagami, *Class. Quantum Grav.* **21**, 3973-3984 (2004).
- [29] R. A. Konoplya, *Phys. Rev.* **D73**, 024009 (2006).
- [30] J.-F. Chang, J. Huang, Y.-G. Shen, *Int. J. Theor. Phys.* **46**, 2617-2625 (2007).
- [31] J. L. Blázquez-Salcedo and C. Knoll, *Phys. Rev.* **D97**, 044020 (2018).
- [32] J. L. Blázquez-Salcedo and C. Knoll, [arXiv: 1811.02014].
- [33] R. A. Konoplya and A. Zhidenko, *Phys. Rev.* **D97**, 084034 (2018).
- [34] O. Klein, *Zeit. für Phys.* **53**, 157 (1929).
- [35] C. Itzykson and J.B. Zuber, *Quantum Field Theory*, McGraw Hill (1980).
- [36] M.I. Katsnelson, K.S. Novoselov, and A.K. Geim, *Nature Physics* **2**, 620 (2006).

TABLE III. Lowest axial massive vectorial (Proca field) quasinormal modes for a Rinaldi black hole with  $r_+ = 10$  (left) and  $r_+ = 100$  (right) produced using the HH method. The multipole number is  $\ell = 1$ . The \* signals the  $\bar{z}_{cI}$  critical value below which the modes are purely imaginary.

$\bar{z}$	$m$	$\omega_R$	$\omega_I$	$N$
0.05	1	$\sim$	-60.7829	80
0.122*	1	$\sim$	-34.1544	90
1	1	-2.8317	-6.0252	80
0.005	2	$\sim$	-542.4367	50
0.032*	2	$\sim$	-128.7811	90
0.05	2	-16.8555	-89.6301	50
0.005	3	$\sim$	-593.9313	90
0.0146*	3	$\sim$	-286.0248	90
0.05	3	-34.0195	-101.6521	50
$\bar{z}$	$m$	$\omega_R$	$\omega_I$	$N$
0.05	1	$\sim$	-603.9213	90
0.133*	1	$\sim$	-315.9499	90
1	1	-26.2228	-60.4218	50
0.005	2	$\sim$	-5420.8095	90
0.033*	2	$\sim$	-1256.5409	90
0.05	2	-162.93768	-897.4394	50
0.005	3	$\sim$	-5935.6459	90
0.0148*	3	$\sim$	-2843.6852	90
0.05	3	-337.4584	-1017.1671	40

TABLE IV. Lowest polar massive vectorial (Proca field) quasinormal modes for a Rinaldi black hole with  $r_+ = 10$  (left) and  $r_+ = 100$  (right) produced using the HH method. The \* signals the  $\bar{z}_{cI}$  critical value below which the modes are purely imaginary.

$\bar{z}$	$m$	$\omega_R$	$\omega_I$	$N$
0.05	1	$\sim$	-4.4840	90
1	1	$\sim$	-2.5320	50
9.6*	1	$\sim$	-1.5014	50
100	1	-0.8276	-0.4266	90
150	1	-0.8325	-0.3495	90
0.05	2	$\sim$	-14.8668	120
1	2	$\sim$	-6.5931	50
3.31*	2	$\sim$	-4.7621	50
100	2	-1.6167	-0.8162	90
150	2	-1.6352	-0.6725	90
$\bar{z}$	$m$	$\omega_R$	$\omega_I$	$N$
0.05	1	$\sim$	-44.8298	90
1	1	$\sim$	-25.0032	50
16.8*	1	$\sim$	-10.0507	50
100	1	-2.2198	-3.6808	50
150	1	-1.8326	-2.9748	50
0.05	2	$\sim$	-148.60705	90
1	2	$\sim$	-64.6226	50
4.25*	2	$\sim$	-39.8864	50
100	2	-4.2949	-7.1127	50
150	2	-3.5728	-5.7916	50



TABLE V. Dirac quasinormal frequencies with fixed horizon radius  $r_+ = 1$  computed using the WKB technique.

$K$	$\sqrt{\bar{z}} = 1$		$\sqrt{\bar{z}} = 0.8$		$\sqrt{\bar{z}} = 0.6$	
	$\omega_R$	$\omega_I$	$\omega_R$	$\omega_I$	$\omega_R$	$\omega_I$
1	0.420	-0.357	0.394	-0.495	0.124	-1.250
2	0.832	-0.340	0.858	-0.410	0.461	-0.776
3	1.273	-0.326	1.361	-0.379	1.290	-0.475
4	1.712	-0.321	1.845	-0.371	1.988	-0.440
5	2.148	-0.319	2.321	-0.369	2.593	-0.450
10	4.315	-0.317	4.679	-0.365	5.458	-0.454
20	8.640	-0.316	9.378	-0.364	10.962	-0.450
50	21.607	-0.3159	23.458	-0.3631	27.439	-0.449